Rheologica Acta (2023) 62:45–55
https://doi.org/10.1007/s00397-022-01380-x

ORIGINAL CONTRIBUTION

Non-linear dilational rheology of liquid-liquid interfaces stabilized by dipeptide hydrogels

Fernando Carbonell-Aviñó[1] · Paul S. Clegg[1]

Received: 14 June 2022 / Revised: 7 October 2022 / Accepted: 1 November 2022 / Published online: 7 December 2022

Abstract
We investigate the effects of salt concentration on the rheological properties of dipeptide hydrogel fibres at liquid-liquid interfaces. The interfaces were subjected to large amplitude oscillatory dilation (LAOD) experiments across a range of oscillation strains and frequencies. Lissajous plots of pressure-strain were used for characterizing the viscoelastic properties and for identifying apparent yielding. We show that key aspects of the rheological response of the interfaces vary significantly with salt concentration. At low strain, independent of salt concentration, Lissajous curves show an almost elliptical shape. As the strain is increased, asymmetry in Lissajous curves evidences a non-linear response. The departure from an ellipse is most obvious at negative strain (at moderate to high salt concentrations) and is suggestive of strain-hardening on compression. The Lissajous curves tilt towards the diagonal at elevated salt concentration demonstrating that the interfaces are becoming increasingly elastic. However, increasing the frequency of the oscillation has little systematic effect. We infer that the addition of salt leads to the development of structure on the interfaces from our observations strain-hardening and of the increasingly elastic response. To fully capture the range of behaviour, we suggest a modification of the analysis to calculate the strain-hardening ratio S used to quantify the degree of non-linearities from Lissajous figures, so as to better reveal the presence of instant strain-softening and strain-hardening responses.

Keywords Interface · Hydrogel · Peptide

Introduction

Emulsions are a crucial design motif for food, personal care, home care and agrochemical products (Tan and McClements 2021; Taylor 1998). To prevent the liquid droplets in the emulsion from coalescing the liquid-liquid interfaces must remain stable during collisions. Furthermore, the detailed flow properties of these interfaces may enhance the droplet lifetime by also suppressing ripening (Bos and Vliet 2001; Dickinson 2001; Bantchev and Schwartz 2003). Long sticky fibres, of nano-scale width, constitute a novel coating for interfaces; the mechanical properties of the interfaces remain to be thoroughly investigated.

✉ Paul S. Clegg
paul.clegg@ed.ac.uk

[1] School of Physics and Astronomy, University of Edinburgh, Peter Guthrie Tait Road, Edinburgh, EH9 3FD, UK

It is well-known that some short sequences of peptides can form hydrogels at low concentration (Jayawarna et al. 2006; Mahler et al. 2006). These molecules and the resulting hydrogels are increasingly being investigated for their capabilities as emulsifiers. Early work on emulsification (and film and foam formation) involved using dipeptides with a protecting group at one end of the molecule (see Fig. 1, inset) (Johnson et al. 2010; Li et al. 2014; Bai et al. 2014; Fleming et al. 2014). An alternative approach, which is becoming increasingly popular, is to avoid this protecting group (Scott et al. 2016; Moreira et al. 2017; Wychowaniec et al. 2020) or to modify it to enhance the emulsification performance (Moreira et al. 2017; Lv et al. 2019). The latter can lead to high performance molecules which are robust when faced with high temperatures or salt concentrations (Lv et al. 2019; De Leon Rodriguez and Hemar 2020). Peptide based emulsifiers also permit a higher level of functionality due to the possibility of triggering or disabling the interfacial activity via the use of an enzyme (Moreira et al. 2016; 2017; Castelletto et al. 2019). Longer peptide sequences with switchable interfacial properties have also

been explored (Dexter et al. 2006; Dexter and Middelberg 2007).

Previous investigations have shown that a tangle of hydrogel fibres exist at the interface (Li et al. 2014). This indicates that the stability of droplets and bubbles is due to a complex composite rather than individual interfacially active molecules. We are interested in the detailed mechanical properties of these composite interfaces so for simplicity, we focus on the canonical simple molecule naphthalene protected diphenylalanine (2NapFF, Fig. 1, inset) (Chen et al. 2010; Li et al. 2016; Avino et al. 2017). We induce gelation via the addition of a salt; the choice of salt has a profound influence on the properties of the 2NapFF hydrogel in bulk (Chen et al. 2011).

The study of the rheological properties of complex interfaces involves the imposition of small area (dilatational rheology) and shape (shear rheology) variations, typically at a known frequency (Miller et al. 1996; Sagis 2011; Erni 2011; Sagis and Fischer 2014). Here we are interested in the mechanical properties of an interfacial layer and we carry out dilatational rheology of an interface using a pendant drop. The volume of the droplet is oscillated at a fixed frequency and the shape of the droplet is measured. By fitting the Young-Laplace equation to the droplet shape both the imposed change in area (i.e. the strain) and the surface pressure response are measured. A good correspondence between the Young-Laplace equation and the droplet shape is essential (Nagel et al. 2017). A sweep of the strain amplitude is usually conducted as a first step to determine the critical strain value beyond which the behaviour of the interface becomes non-linear (van Kempen et al. 2013). Once this is known, the properties of the interface can be further interrogated by applying frequency sweeps in the linear and/or non-linear regimes.

In Refs. Rühs et al. (2013a, b) and van Kempen et al. (2013), Lissajous plots were employed to analyse amplitude sweeps for interfacial dilatational rheology studies. Strain moduli characteristic of the full plot were developed to draw out quantitative details from the data. While this works excellently under many circumstances, contradictions are known to occur whereby the data from a strain-softening material appear to indicate strain-hardening on a Lissajous plot (Mermet-Guyennet et al. 2015).

In this paper, the effect of salt concentration on the mechanical properties of interfaces stabilized by dipeptide fibres is investigated by imposing large amplitude oscillatory dilatational (LAOD) deformations on interfaces using a drop profile tensiometer. We find that non-linearities appear at intermediate and high strain amplitudes, while frequency does not have a significant influence. Interfaces prepared at intermediate salt concentrations, exhibit a viscoelastic response. At the highest salt concentration, interfaces are elastic but yield at low deformations, implying that they have become brittle. Finally, we suggest a modification of the analysis for quantifying non-linearities from Lissajous plots, based on instantaneous strain moduli, to better reveal the presence of strain-softening and strain-hardening responses.

Experimental

Materials

The 2NapFF dipeptides were synthesized at the University of Glasgow as described elsewhere (Chen et al. 2010). The solvents and chemicals were purchased from Sigma-Aldrich. Isopropyl myristate (Sigma-Aldrich ≥ 98 % pure) was filtered three times through alumina powder (Honeywell, Aluminium Oxide, activated, basic, Brockmann I) prior to use in order to remove polar impurities. A solution of 100 mL (1M) magnesium sulfate was dissolved

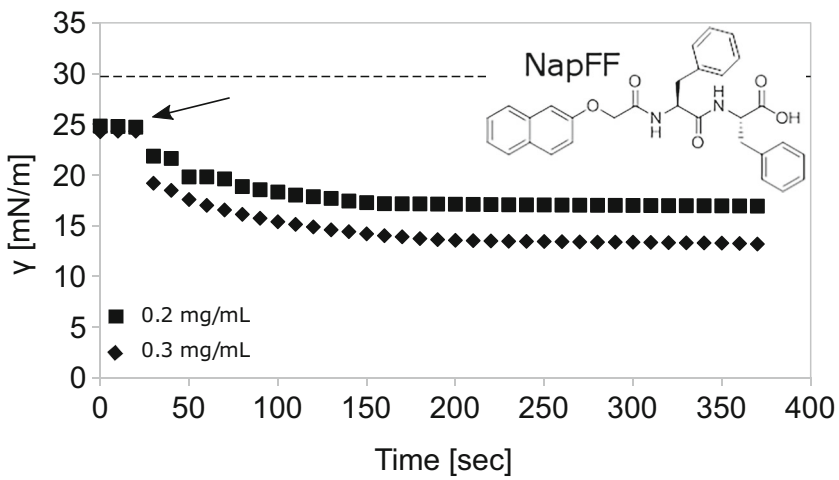

Fig. 1 Interfacial tension, γ, of interfaces prepared using 0.01 wt% 2NapFF. Oil droplets are left unperturbed until the interfacial tension reaches equilibrium. The black arrow indicates the addition of salt. The dashed line is γ of a clean isopropyl myristate-Milli-Q water interface. Inset: Naphthalene dipeptide molecules used in this study

in water and used as aliquots. Millipore water (resistivity 18.2 MΩ cm) was used throughout. For pendant drop experiments water was degassed by heating and stirring under reduced pressure for one hour to avoid bubbles disrupting oscillations.

Methods

Samples were prepared in 20-mL glass vials by adding 10 mM of NaOH to 10 mL of degassed water to achieve a pH 11 ± 0.5 measured with a Seven Easy pH probe (Mettler Toledo AG). 2NapFF dipeptides (0.01 wt%) were then added on top of the basic solution and dispersed by placing the vial sealed with film (Parafilm) in an ultrasonic bath for 0.5 hours until a translucent slightly viscous solution was formed. After this, the sample was then left to cool to room temperature (22 °C) before being transferred to a 36 × 36 × 30 mm^3 glass cuvette.

Apparatus validation The droplet volume influences the accuracy of the pendant drop tensiometer (Krüss Easy Drop, Krüss GmbH, Germany) because spherical droplets yield inconsistent results (Hoorfar and Neumann 2006). To avoid this, we increased the volume of the oil droplet until the interfacial tension of the bare interface equilibrated to a value of 29 mN/m which compares favourably with literature values (Binks et al. 2010). The final volume was 25 µL. The second stage-gate is the quality of the fit to the Young-Laplace equation. After optimization is complete, the software shows the mean squared deviation of the profile from the fit to the model. A high fit error, in the range of tens or hundreds of microns, is associated with solidifying interfaces, where wrinkles are observed in compressed interfacial films (Hegemann et al. 2018). A clean isopropyl myristate/water interface gives a fit error < 1 µm and thus experiments with fit errors ≥ 1 µm were rejected. Next, we verify that the subphase contributions do not dominate over interfacial stresses by calculating the Boussinesq number (Erk et al. 2012; Brenner 2013; Mears 2020) using $Bq = E/\omega\nu L$. For the smallest interfacial dilational modulus E = 0.05 mN/m, and the highest frequency = 0.2 Hz we find a $Bq > 10^2$ (for the drop length scale L = 1 mm with the viscosity of isopropyl myristate as ν = 1.02 mPa s at 20 °C) indicating the interfacial dilational elasticity dominates.

Experiment setup After a deep cleaning of the instrument parts with hexane, followed by methanol and rinsing with Millipore water, the instrument was tested by placing Millipore water in the cuvette and forming an air bubble with a J-shaped needle to achieve an interfacial tension of 72 ± 0.5 mN/m at 22 °C. Next, the syringe was filled with isopropyl myristate and a droplet of 25 µL formed with interfacial tension comparable to γ = 29 ± 0.5 mN/m at 22 °C. Then the water in the cuvette was replaced by the basic solution of dispersed dipeptides. To equilibrate the solution, we again form the oil droplet and let it rest (≈ 5 minutes); γ drops rapidly (< 1 second) from ≈ 29 mN/m to ≈ 25 mN/m (data not shown). Now aliquots of different salt concentrations (0.1 mg/mL, 0.2 mg/mL, 0.3 mg/mL and 0.4 mg/mL) were added on top of the sample to induce film gelation. Finally, the cuvette was covered with a lid to minimize evaporation.

The surface tension of an interfacial film from a static droplet was measured before, during and after the addition of salt and left until the sample reached equilibrium (≈ 5 hours). Then the surface tension was recorded during amplitude and frequency sweep experiments to study the non-linear response of the complex interfaces. During the sweep tests, sinusoidal oscillations with a strain amplitude and frequency that increased from 1.5% to 25% and 0.02 Hz to 0.2 Hz respectively were performed. The experiments consisted of 20 cycles of oscillations with 5 minutes rest between experiments. The initial and final cycles were removed from the analysis to eliminate the influence of potential outliers. Outliers were also removed from the raw data in both axis (x, y) and smoothing was carried out via a running average of point pairs.

Describing the data

Outside the linear regime, physical meaning can be extracted from the Lissajous plots formed by plotting the pressure as a function of strain. For a perfect elastic solid, the Lissajous plot shows a straight line, for a pure viscous response a perfect circle is found and for a linear viscoelastic fluid the plot is an ellipse. Such plots have been used in bulk LAOS experiments to study the rheological properties of viscoelastic materials in the non-linear regime including, polymer solutions (Philippoff 1966), creams (Davis 1971) and clay-water systems (Payne and Whittaker 1971; Krizek 1971). Ewoldt et al. (2008) introduced a set of elastic moduli in order to quantify the response of non-linear viscoelastic materials at large shear strains. To characterize non-linearities distorting the ellipse, these authors defined the shear strain-hardening ratio S where $S < 0$ indicates strain-softening, $S > 0$ implies strain-hardening and $S = 0$ denotes an elastic response. Ewoldt's approach to calculate the *S–factor*, was later extended by others (van Kempen et al. 2013; Rühs et al. 2013a) to characterize the response of air-water interfaces in LAOD deformations. Here the pressure is defined as:

$$\Pi = \gamma - \gamma_0 \tag{1}$$

where γ is the tension of the interface and γ_0 is the tension of the non deformed interface. Due to the asymmetry in the

Lissajous plots during a full cycle, the strain-hardening ratio S is defined for both extension and compression as:

$$S_{ext} \equiv \frac{E_{L,E} - E_{M,E}}{E_{L,E}} \quad (2)$$

$$S_{com} \equiv \frac{E_{L,C} - E_{M,C}}{E_{L,C}} \quad (3)$$

where $E_{L,E}$ and $E_{M,E}$ is the large and minimum strain modulus upon extension and $E_{L,C}$ and $E_{M,C}$ upon compression (see Ref. van Kempen et al. 2013, Fig. 2).

Results and discussion

The interfacial tension γ of interfaces stabilized by dipeptide fibres (2NapFF) at 0.2 mg/mL and 0.3 mg/mL magnesium sulfate was measured first during dipeptide adsorption and subsequently after the addition of salt. Here the quantities of dipeptide are small compared to those required to create a bulk hydrogel. In the absence of salt, spherical micelles are expected at 0.01 wt% 2NapFF (Cardoso et al. 2016). The addition of salt leads to both the formation of fibres and, potentially, gelation on the interface (Li et al. 2014; Avino et al. 2017). γ for a isopropyl myristate-Milli-Q water interface is $\approx$ 29.7 mN/m at 22 °C and decreases to $\approx$ 25 mN/m due to the presence of dipeptide. After addition of salt, γ decreases slowly to $\approx$ 16.5 mN/m and $\approx$ 13.5 mN/m for interfaces prepared at 0.2 mg/mL and 0.3 mg/mL respectively, Fig. 1. After 5 h, interfaces reach equilibrium and are ready for oscillation.

Lissajous plots

The effect of salt on the mechanical properties of oil-water interfaces stabilized by dipeptide fibres (2NapFF), was investigated by imposing large amplitude oscillatory dilatational (LAOD) frequency and strain sweeps on the oil droplets. We begin by looking at the low salt case as our baseline for comparison. The surface pressure of interfaces prepared at 0.1 mg/mL magnesium sulfate oscillated at 0.02 Hz and 1.5% strain is below the detection limit of the apparatus (see Fig. 2a). At higher strain (8%), the data is still a bit scattered in the plateau region of the pressure-strain curve, however, the curve is a horizontal ellipse indicative of a viscous interface (Fig. 2b). With increasing frequency (Fig. S1), the noise decreases and Lissajous ellipses become wider and slightly tilted, characteristic of the interfaces becoming increasingly viscoelastic.

At 16% Lissajous curves become asymmetric due to a noticeably non-linear response from the interfaces (see Fig. 2c). At positive strains, the curve remains indicative of viscous flow. Intriguingly, we observe secondary oscillations (see black arrow in Fig. 2c) corresponding to several distinct strains being associated with the same pressure; this has previously been observed in interfacial rheology studies (see Figure 10 in Ref. Sagis et al. (2014)). At negative strains, there is a noticeable start of an asymmetric response, suggestive of strain-hardening on compression. This evidences increasing structure on the interface. Lissajous curves from interfaces oscillated at higher frequencies (Fig. S2), share similarities with Fig. 2c but, they become wider and more tilted with increasing frequency. At the highest frequency irregular fluctuations come to dominate (Fig. S2).

Next we consider the effect of increasing the salt concentration. Figure 3 shows the Lissajous curves of interfaces prepared at (left panel) 0.2 mg/mL, (middle panel) 0.3 mg/mL and (right panel) 0.4 mg/mL magnesium sulfate oscillated at 0.02 Hz and (first row) 8%, (second row) 16% and (third row) 25% strain. At 8% strain (Fig. 3a, b, c) all Lissajous curves are quite noisy but show a close to perfect ellipse, suggesting they reflect linear response. Interfaces oscillated at 16% and 25% show relatively horizontal major axes at salt concentrations 0.2 mg/mL and 0.3 mg/mL with the major axis tilting closer to the diagonal for 0.4 mg/mL (Fig. 3d–i). This tilting corresponds to an increase in the elastic response clearly indicating that at elevated salt concentration there is interfacial structure that resists extension. It is noticeable that both Fig. 3a and Fig. 3c are also somewhat tilted.

At first sight, Fig. 3d, e, g and h are reminiscent of the low salt case presented in Fig. 2b, c, however, there is strain-softening on extension when beginning from maximum compression and an onset of strain-hardening approaching the maximum extension at 0.3 mg/mL (red arrows, Fig. 3e, h). By contrast, there is more pronounced strain-hardening on compression at 0.4 mg/mL (most clearly in Fig. 3i). Here, the maximum surface pressure observed on compression is significantly higher than that for extension. Secondary oscillations are visible on compression in both Fig. 3f and h (black arrows).

Interfaces oscillated at higher frequencies (Fig. S3), do not lose the elliptical shape when deformed at 8%, but become wider and more tilted, which indicates interfaces with higher viscoelastic moduli. At 16% strain, the pressure increases with increasing frequency for interfaces prepared at 0.2 mg/mL, but barely changes the shape of the Lissajous curves (Fig. S4a, b). On the other hand, at higher salt concentrations (Fig. S4c–g), the increase in frequency seems to have a greater effect. At 0.3 mg/mL and 0.4 mg/mL the pressure increases in extension and in compression, hence forming wider Lissajous curves. For 25% (Fig. S5), the increase in frequency only has a modest affect on the shape of the Lissajous curves. Across all frequencies and most amplitudes, we see a strain-hardening kink on

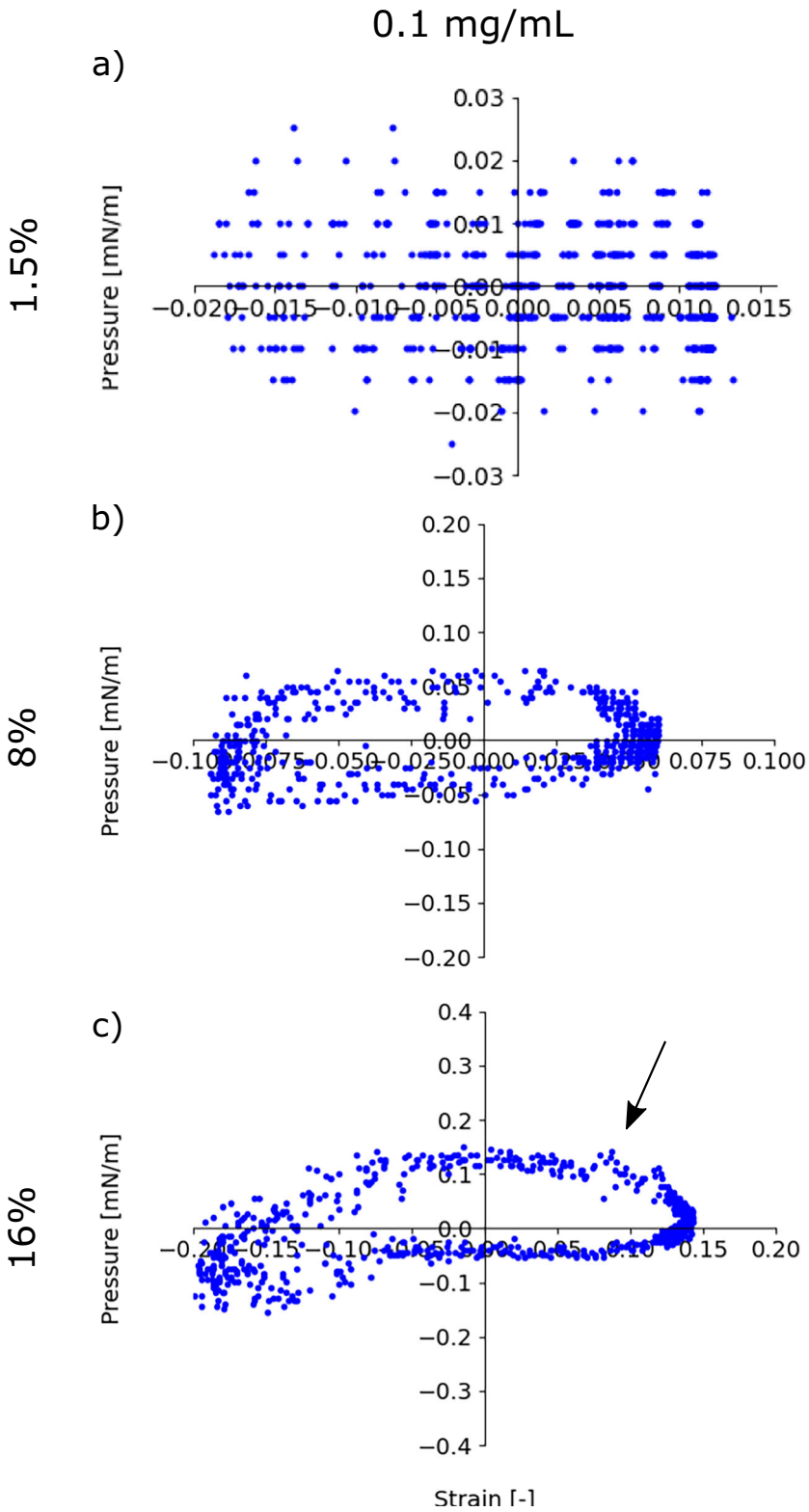

Fig. 2 Lissajous plots obtained during amplitude sweeps (a) 1.5%, (b) 8% and (c) 16% of an interface made of 0.01 wt% 2NapFF prepared at 0.1 mg/mL magnesium sulfate, oscillated at a fixed frequency (0.02 Hz). Black arrow indicates secondary oscillations

extension at 0.3 mg/mL which gives way to a more tilted ellipse and more profound strain-hardening on compression at 0.4 mg/mL. These trends show that the addition of salt leads to the development of structure on the interface which contributes a marked strain-hardening aspect to the response.

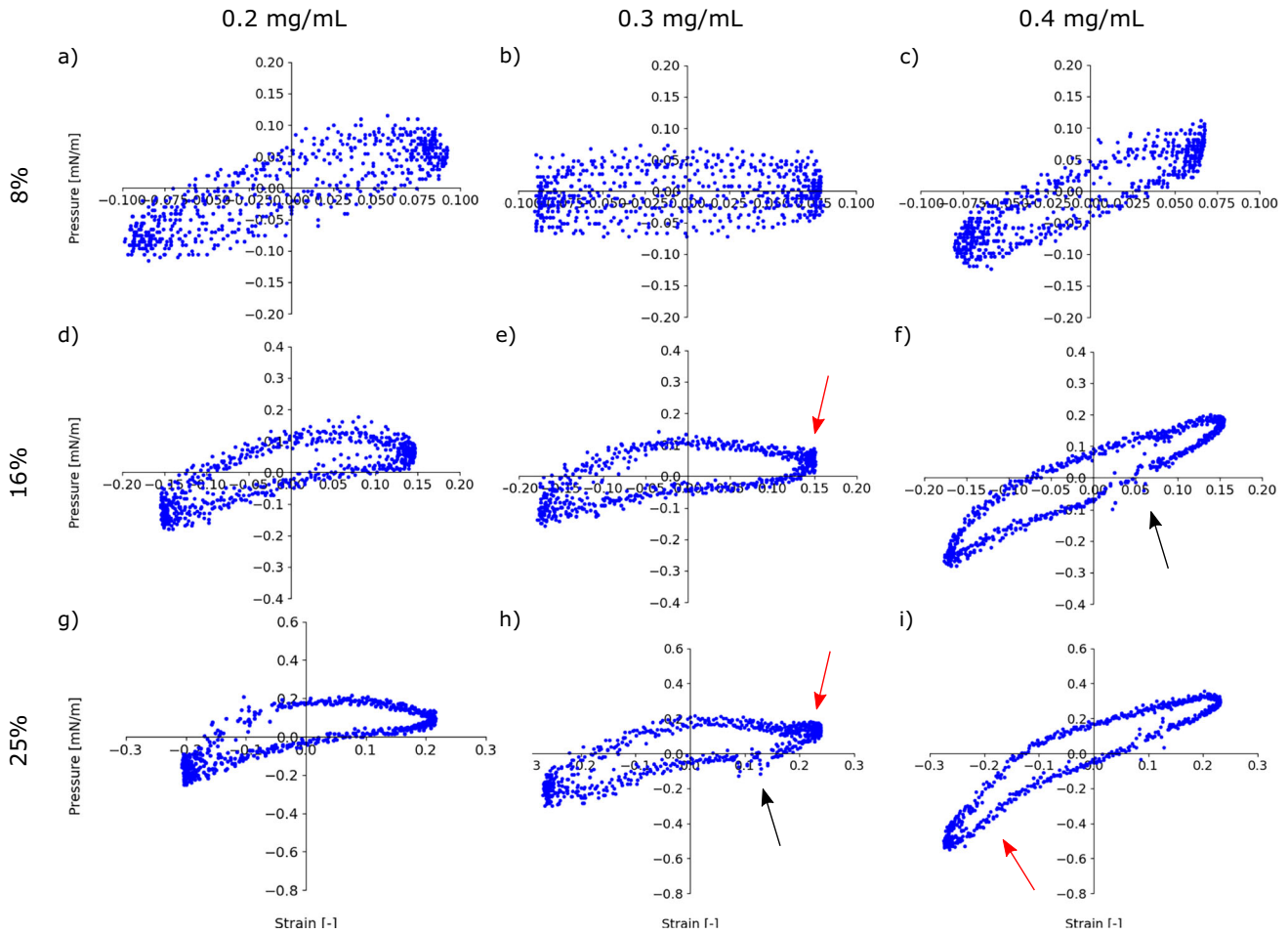

Fig. 3 Lissajous plots obtained during amplitude sweeps (8–25%) of interfaces made of 0.01 wt% 2NapFF prepared at different salt concentrations (0.2–0.4 mg/mL), oscillated at a fixed frequency (0.02 Hz). Black and red arrows indicate secondary oscillations and strain-hardening respectively

Quantifying the degree of non-linearities from Lissajous plots

Non-linearities in Lissajous plots can be quantified using the strain-hardening ratio *S* (*S–factor*), Eqs. 2 and 3. An *S–factor* with a value close to zero is indicative of interfaces with linear elastic response; negative or positive values correspond to strain-softening or strain-hardening responses respectively. Figure 4a shows the *S–factor* of Lissajous plots for the interface prepared at 0.1 mg/mL (Fig. 2) with the scattered data for the lowest amplitude suppressed. At 8% strain, the *S–factor* is positive and increases in extension and in compression with increasing strain amplitude, implying a strain-hardening response.

The *S–factor* of Lissajous plots for interfaces prepared at 0.2–0.4 mg/mL (Fig. 3) is presented in Fig. 4b, c, d. At 0.2 mg/mL the *S–factor* is negative on extension at 8% and 16%, but becomes positive at 25%, which suggests an interface with a strain-softening response at low and intermediate deformations and with a strain-hardening response at higher deformations. In compression, we observe a positive *S–factor* increasing non-monotonically, being close to zero at 8% and reaching its maximum value at 16%. At 25% this decreases slightly implying that, the strain-hardening response decreases at high deformations after reaching its maximum value at intermediate deformations. The *S–factor* from the interface prepared at 0.3 mg/mL oscillated at 8% was not calculated because the noise was still too high even after smoothing the data. At 16%, the *S–factor* is positive on extension and compression and decreases slightly for interfaces oscillated at 25%, indicating an interface with a higher strain-hardening response in extension and compression at intermediate deformations. Lastly, Lissajous curves from interfaces prepared at 0.4 mg/mL, show a positive but low *S–factor* in extension and in compression. In extension, this is higher in interfaces oscillated at 8% and 25%, suggesting a less strain-hardening interface at intermediate deformations. However, in compression, the *S–factor* is close to zero in extension at 8% and 16% and increases at 25%, implying an interface with an elastic response at low and intermediate deformations in compression.

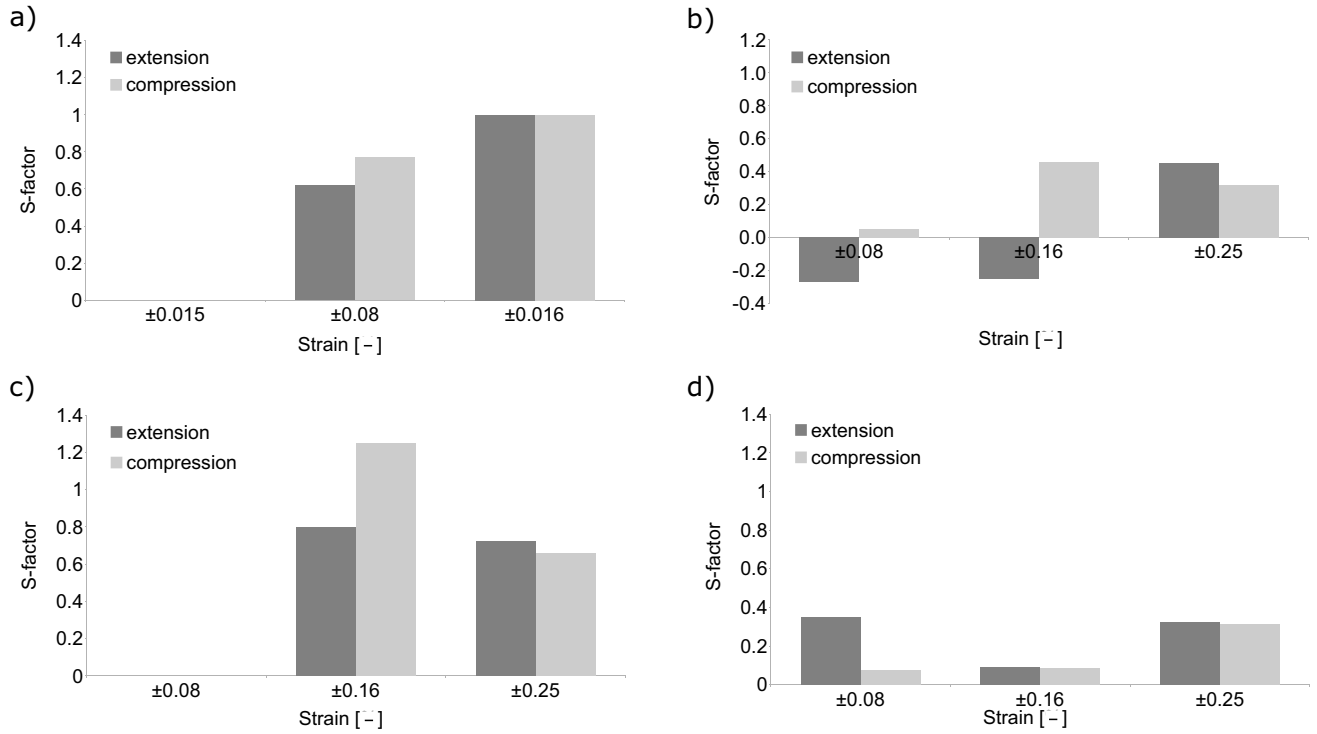

Fig. 4 S–factor obtained from Lissajous plots during amplitude sweeps (1.5–25%) of interfaces made from 0.01 wt% 2NapFF prepared at (a) 0.1 mg/mL and (b) 0.2 mg/mL, (c) 0.3 mg/mL, (d) 0.4 mg/mL magnesium sulfate, oscillated at a fixed frequency (0.02 Hz). A *S–factor* with a value close to zero indicates an interface with an elastic response, whereas a *S–factor* with a positive or negative value corresponds to an interface with a strain-hardening and strain-softening response respectively

Analysing the *S–factor*, we find that this contradicts the Lissajous curves to some extent. Peak strain-hardening is shown at 0.1 and 0.3 mg/mL (Fig. 4) in contrast to the relatively monotonic evolution of the Lissajous curves. Furthermore, Lissajous plots show some strain-softening in extension for interfaces oscillated at 16% and 25%, which is particularly clear when starting from maximum compression, the *S–factor* is often positive. This phenomena was first reported by Ma et al. (1999) when studying the micro-mechanical properties of a keratin filament network, using strain-controlled rheometry. However, it was not until Ewoldt et al. (2008) introduced a framework to interpret non-linearities physically in the response to imposed LAOS deformations, that this issue was raised. In this work they focus on the local behaviour represented by the Lissajous curves and hence systems are reported to be strain-hardening. Subsequently Mermet-Guyennet et al. (2015) realized that, even if the viscoelastic modulus decreases in the non-linear regime with increasing deformation for a large number of soft materials, they still are usually reported as showing a strain-hardening response when analysed via Lissajous curves. They called this phenomena the strain-softening/strain-hardening paradox after demonstrating that the strain-hardening response observed is local due to the use of a tangent modulus in the LAOS analysis that increases with increasing deformation and by showing that the strain-softening is the dominant effect, and hence the overall response as shown by the change in slope of the minimum strain modulus G_M.

New approach to quantify non-linearities

In the previous Section we addressed the differences between the Lissajous plots from Figs. 2 and 3 and the *S–factor* from Fig. 4. Here, we suggest a modification to the analysis to quantify non-linearities from Lissajous plots that reveals better the presence of strain-softening and strain-hardening responses. We replace the minimum strain modulus E_M in Eqs. 2 and 3 by the slope of the instantaneous strain modulus E sampled at a subset of points (here alternate points from a single cycle) to give,

$$s_{ext} \equiv \frac{E - E_{L,E}}{E_{L,E}} \tag{4}$$

$$s_{com} \equiv \frac{E - E_{L,C}}{E_{L,C}} \tag{5}$$

The signs in the numerator have been chosen to preserve the interpretation of the sign of the *s–factor*. Figure 5 shows the evolution of the *s–factor* of Lissajous curves

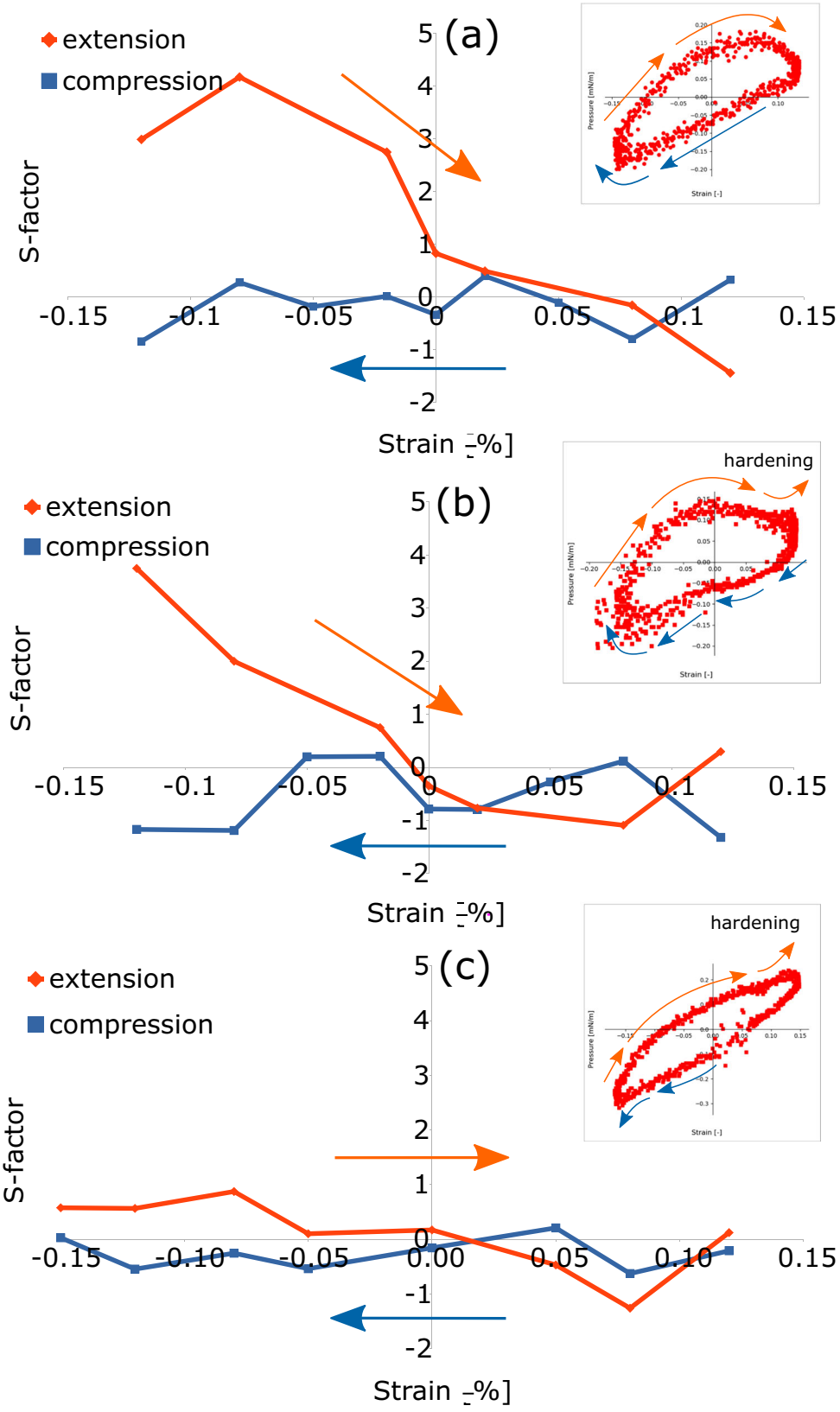

Fig. 5 Evolution of the *s–factor* from Lissajous plots of interfaces made of 0.01 wt% 2NapFF oscillated at 0.05 Hz and 16%, prepared at (a) 0.2 mg/mL, (b) 0.3 mg/mL and (c) 0.4 mg/mL magnesium sulfate. The arrows indicate the direction of the cycle (expansion and compression). Insets show Lissajous plots of interfaces being characterized. The arrows in insets are placed to aid the eye with the interface response and to indicate the direction of the cycle. This form of analysis emphasizes the steady evolution of the interfacial properties with increasing salt concentration

from interfaces prepared at 0.2 mg/mL, 0.3 mg/mL and 0.4 mg/mL magnesium sulfate oscillated at a frequency of 0.05 Hz and 16% strain.

The *s–factor* from a Lissajous curve of an interface prepared at 0.2 mg/mL in extension, is positive at negative strains (Fig. 5a). These results indicate that at the start of extension the interface shows an initial strain-hardening response, however, this becomes strain-softening as the strain increases. In compression, the interface shows a more elastic response, observed by the *s–factor* barely changing and being close to zero.

The evolution of the *s–factor* from a Lissajous plot of an interface prepared at 0.3 mg/mL (Fig. 5b) is somewhat similar. The *s–factor* for extension is positive at negative strains, but decreases fast with increasing strain. At a strain near zero, this reaches zero and decreases further until a strain $\approx$ +0.08, where it reaches its minimum value. At higher strains, the *s–factor* increases and becomes strain-hardening by the end of extension. In compression, the *s–factor* is more varied than that for an interface prepared at 0.2 mg/mL with an overall tendency towards strain-softening.

At 0.4 mg/mL, the *s–factor* again starts positive in extension (Fig. 5c), however, the values are far lower than for interfaces prepared at 0.2 mg/mL and 0.3 mg/mL. This suggests that the interface prepared at 0.4 mg/mL has a more elastic response than interfaces prepared at lower salt concentrations. Similar to interfaces prepared at 0.3 mg/mL, the *s–factor* increases and becomes slightly positive by the end of extension. In compression, the *s–factor* barely changes and is close to zero. Overall, Fig. 5 shows a more clear progression with salt concentration and a more realistic reflection of the Lissajous curves.

Conclusions

In this paper we have investigated the effect of salt concentration on the rheological properties of salt-induced hydrogel films made of 2NapFF. Interfaces were subjected to strain and frequency sweeps in the linear and non-linear viscoelastic regime via the oscillating drop technique. Plotting pressure-strain curves from interfaces subjected to LAOD deformations as Lissajous curves has allowed us to analyse the rheological response of the interfaces beyond the linear regime.

All interfaces showed Lissajous curves with an almost elliptical shape at 8% strain, which indicates that these are still within the linear regime. Asymmetric Lissajous curves from 16% strain indicates that the interfaces are now in the non-linear regime. This is most noticeable, at negative strains, where the shape is suggestive of strain-hardening on compression. This evidences increasing structure on the interface. Interfaces prepared at 0.4 mg/mL salt showed the highest elastic response of all interfaces, with the pressure still increasing after these have yielded and very pronounced strain-hardening on compression (especially at 25% strain). By contrast, increasing the frequency did not have a significant effect on the properties of the interfaces compared to the strain. From the increasingly elastic character and the strain-hardening response, we infer that the addition of salt leads to the development of structure on the interface.

Finally, we and other authors (Mermet-Guyennet et al. 2015; Giménez-Ribes et al. 2020; Precha-Atsawanan et al. 2018) realized that the strain-hardening ratio *S* or *S–factor* used to quantify non-linearities from Lissajous plots, can sometimes give misleading measures. We suggest using the instantaneous strain elastic moduli E rather than the minimum strain elastic moduli E_M in Eqs. 2 and 3, to capture the overall response of the interfaces, regardless of which response (elastic or viscous) dominates.

Supporting information This file contains additional figures of Lissajous plots from interfaces oscillated at higher frequencies (0.05 Hz, 0.1 Hz and 0.2 Hz).

Supplementary information The online version contains supplementary material available at https://doi.org/10.1007/s00397-022-01380-x.

Acknowledgements We thank D.J. Adams for providing the 2NapFF dipeptides. For the purpose of open access, the author has applied a Creative Commons Attribution (CC BY) licence to any Author Accepted Manuscript version arising from this submission.

Funding FC-A received a studentship funded by the EPSRC (EP/N509644/1).

Declarations

Conflict of interest The authors declare no competing interests.

References

Avino F, Matheson AB, Adams DJ, Clegg PS (2017) Long-lived foams stabilized by a hydrophobic dipeptide hydrogel. Organic Biomol Chem 15:6342–6348

Bai S, Pappas C, Debnath S, Frederix PW, Leckie J, Fleming S, Ulijn RV (2014) Stable emulsions formed by self-assembly of interfacial networks of dipeptide derivatives. ACS Nano 8:7005–7013

Bantchev GB, Schwartz DK (2003) Surface shear rheology of β-casein layers at the air/solution interface: formation of a two-dimensional physical gel. Langmuir 19:2673–2682

Binks BP, Fletcher PD, Holt BL, Parker J, Beaussoubre P, Wong K (2010) Drop sizes and particle coverage in emulsions stabilised solely by silica nanoparticles of irregular shape. Phys Chem Chem Phys 12:11967–11974

Bos MA, Vliet TV (2001) Interfacial rheological properties of adsorbed protein layers and surfactants: a review. Adv Colloid Interface Sci 91:437–471

Brenner H (2013) Interfacial transport processes and rheology. Elsevier, Amsterdam

Cardoso AZ, Mears LL, Cattoz BN, Griffiths PC, Schweins R, Adams DJ (2016) Linking micellar structures to hydrogelation for salt-triggered dipeptide gelators. Soft Matter 12:3612–3621

Castelletto V, Edwards-Gayle CJ, Hamley IW, Barrett G, Seitsonen J, Ruokolainen J (2019) Peptide-stabilized emulsions and gels from an arginine-rich surfactant-like peptide with antimicrobial activity. ACS Appl Mater Interfaces 11:9893–9903

Chen L, Revel S, Morris K, Serpell LC, Adams DJ (2010) Effect of molecular structure on the properties of naphthalene-dipeptide hydrogelators. Langmuir 26:13466–13471

Chen L, Pont G, Morris K, Lotze G, Squires A, Serpell LC, Adams DJ (2011) Salt-induced hydrogelation of functionalised-dipeptides at high pH. Chem Commun 47:12071–12073

Davis SS (1971) Viscoelastic properties of pharmaceutical semisolids IV: Destructive oscillatory testing. J Pharm Sci 60:1356–1360

De Leon Rodriguez LM, Hemar Y (2020) Prospecting the applications and discovery of peptide hydrogels in food. Trends Food Sci Technol 104:37–48

Dexter AF, Middelberg AP (2007) Switchable peptide surfactants with designed metal binding capacity. J Phys Chem C 111:10484–10492

Dexter AF, Malcolm AS, Middelberg AP (2006) Reversible active switching of the mechanical properties of a peptide film at a fluid–fluid interface. Nat Mater 5:502–506

Dickinson E (2001) Milk protein interfacial layers and the relationship to emulsion stability and rheology. Colloids Surf B Biointerfaces 20:197–210

Erk KA, Martin JD, Schwalbe JT, Phelan JrFR, Hudson SD (2012) Shear and dilational interfacial rheology of surfactant-stabilized droplets. J Colloid Interface Sci 377:442–449

Erni P (2011) Deformation modes of complex fluid interfaces. Soft Matter 7:7586–7600

Ewoldt RH, Hosoi A, McKinley GH (2008) New measures for characterizing nonlinear viscoelasticity in large amplitude oscillatory shear. J Rheol 52:1427–1458

Fleming S, Debnath S, Frederix PW, Hunt NT, Ulijn RV (2014) Insights into the coassembly of hydrogelators and surfactants based on aromatic peptide amphiphiles. Biomacromol 15:1171–1184

Giménez-Ribes G, Habibi M, Sagis LM (2020) Interfacial rheology and relaxation behavior of adsorption layers of the triterpenoid saponin Escin. J Colloid Interface Sci 563:281–290

Hegemann J, Knoche S, Egger S, Kott M, Demand S, Unverfehrt A, Rehage H, Kierfeld J (2018) Pendant capsule elastometry. J Colloid Interface Sci 513:549–565

Hoorfar M, Neumann A (2006) Recent progress in axisymmetric drop shape analysis (ADSA). Adv Colloid Interface Sci 121:25–49

Jayawarna V, Ali M, Jowitt TA, Miller AF, Saiani A, Gough JE, Ulijn RV (2006) Nanostructured hydrogels for three-dimensional cell culture through self-assembly of fluorenylmethoxycarbonyl-dipeptides. Adv Mater 18:611–614

Johnson EK, Adams DJ, CP J (2010) Directed self-assembly of dipeptides to form ultrathin hydrogel membranes. J Am Chem Soc 132:5130–5136

van Kempen SE, Schols HA, van der Linden E, Sagis LM (2013) Non-linear surface dilatational rheology as a tool for understanding microstructures of air/water interfaces stabilized by oligofructose fatty acid esters. Soft Matter 9:9579–9592

Krizek RJ (1971) Rheologic behavior of clay soils subjected to dynamic loads. Trans Soc Rheol 15:433–489

Li T, Kalloudis M, Cardoso AZ, Adams DJ, Clegg PS (2014) Drop-casting hydrogels at a liquid interface: the case of hydrophobic dipeptides. Langmuir 30:13854–13860

Li T, Nudelman F, Tavacoli JW, Vass H, Adams DJ, Lips A, Clegg PS (2016) Long-lived foams stabilized by a hydrophobic dipeptide hydrogel. Adv Mater Interfaces 3:1500601

Lv W, Hu T, Taha A, Wang Z, Xu X, Pan S, Hu H (2019) Lipo-dipeptide as an emulsifier: performance and possible mechanism. J Agric Food Chem 67:6377–6386

Ma L, Xu J, Coulombe PA, Wirtz D (1999) Keratin filament suspensions show unique micromechanical properties. J Biol Chem 274(27):19145–19151

Mahler A, Reches M, Rechter M, Cohen S, Gazit E (2006) Rigid, self-assembled hydrogel composed of a modified aromatic dipeptide. Adv Mater 18:1365–1370

Mears R (2020) Structure and mechanical properties of model colloids at liquid interfaces. The University of Edinburgh

Mermet-Guyennet M, Gianfelice de Castro J, Habibi M, Martzel N, Denn M, Bonn D (2015) Laos: the strain softening/strain hardening paradox. J Rheol 59:21–32

Miller R, Wüstneck R, Krägel J, Kretzschmar G (1996) Dilational and shear rheology of adsorption layers at liquid interfaces. Colloids Surf A Physicochem Eng Asp 111:75–118

Moreira IP, Sasselli IR, Cannon DA, Hughes M, Lamprou DA, Tuttle T, Ulijn RV (2016) Enzymatically activated emulsions stabilised by interfacial nanofibre networks. Soft Matter 12:2623–2631

Moreira IP, Piskorz TK, van Esch JH, Tuttle T, Ulijn RV (2017) Biocatalytic self-assembly of tripeptide gels and emulsions. Langmuir 33:4986–4995

Nagel M, Tervoort TA, Vermant J (2017) From drop-shape analysis to stress-fitting elastometry. Adv Colloid Interface Sci 247:33–51

Payne A, Whittaker R (1971) Low strain dynamic properties of filled rubbers. Rubber Chem Technol 44:440–478

Philippoff W (1966) Vibrational measurements with large amplitudes. Trans Soc Rheol 10:317–334

Precha-Atsawanan S, Uttapap D, Sagis LM (2018) Linear and nonlinear rheological behavior of native and debranched waxy rice starch gels. Food Hydrocoll 85:1–9

Rühs PA, Affolter C, Windhab EJ, Fischer P (2013a) Shear and dilatational linear and nonlinear subphase controlled interfacial rheology of β-lactoglobulin fibrils and their derivatives. J Rheol 57:1003–1022

Rühs PA, Scheuble N, Windhab EJ, Fischer P (2013b) Protein adsorption and interfacial rheology interfering in dilatational experiment. Eur Phys J Special Top 222:47–60

Sagis L (2011) Dynamic properties of interfaces in soft matter: experiments and theory. Rev Mod Phys 83:1367–1403

Sagis L, Fischer P (2014) Nonlinear rheology of complex fluid–fluid interfaces. Curr Opin Colloid Interface Sci 19:520–529

Sagis L, Humblet-Hua K, Van Kempen S (2014) Nonlinear stress deformation behavior of interfaces stabilized by food-based ingredients. J Phys Condens Matter 26:464105

Scott GG, McKnight PJ, Tuttle T, Ulijn RV (2016) Tripeptide emulsifiers. Adv Mater 28:1381–1386

Tan C, McClements DJ (2021) Application of advanced emulsion technology in the food industry: a review and critical evaluation. Foods 10:812

Taylor P (1998) Ostwald ripening in emulsions. Adv Colloid Interface Sci 75:107–163

Wychowaniec JK, Patel R, Leach J, Mathomes R, Chhabria V, Patil-Sen Y, Hidalgo-Bastida A, Forbes RT, Hayes JM, Elsawy MA (2020) Aromatic stacking facilitated self-assembly of ultrashort ionic complementary peptide sequence: β-sheet nanofibers with remarkable gelation and interfacial properties. Biomacromol 21:2670–2680